Solid Freeform Fabrication 2017: Proceedings of the 28th Annual International Solid Freeform Fabrication Symposium – An Additive Manufacturing Conference
Reviewed Paper

Optimization of Build Orientation for Minimum Thermal Distortion in DMLS Metallic Additive Manufacturing

Authors: Hao Peng[1], Morteza Ghasri-Khouzani[2], Shan Gong[2], Ross Attardo[3], Pierre Ostiguy[3], Bernice Aboud Gatrell[3], Joseph Budzinski[3], Charles Tomonto[3], Joel Neidig[4], M. Ravi Shankar[2], Richard Billo[5], David B. Go[1,6], David Hoelzle[7]

1. Dept. of Aerospace and Mechanical Engineering, University of Notre Dame
2. Dept. of Industrial Engineering, University of Pittsburgh
3. Johnson & Johnson Co.
4. ITAMCO
5. Dept. of Computer Science, University of Notre Dame
6. Dept. of Chemical and Biomolecular Engineering, University of Notre Dame
7. Dept. of Mechanical and Aerospace Engineering, The Ohio State University

Abstract

The additive manufacturing (AM) process direct metal laser sintering (DMLS) can quickly produce complex parts. However, thermal stress in DMLS may induce thermal distortion and cause build failure. This manuscript presents an optimization algorithm for the build orientation in DMLS to minimize thermal distortion. The algorithm is built on the foundation of two coupled thermal and thermo-mechanical models developed in our previous work. The DIRECT search method and a universal objective function for thermal distortion were used. Constraints were included to rule out build orientations resulting in overheating or excessive oxidation. The optimization algorithm was tested on a rectangular bar and a complex, contoured part. Both parts were printed using an EOS M290 machine, and measured by a coordinate measuring machine. In comparison to build orientations chosen by two novice operators, the optimized build orientations gave significant reduction in the thermal distortion and number of print trials before print success.

Keywords: additive manufacturing, DMLS, optimization, build orientation, thermal distortion, thermal stress, support structure

1. Introduction

This manuscript presented an optimization algorithm which minimizes thermal distortion in the metal powder bed fusion (PBF) additive manufacturing (AM) tool Direct Metal Laser Sintering (DMLS) [1] by using an optimal build orientation. DMLS, as schematically shown in Fig. 1, uses a layer-by-layer build cycle to build three-dimensional (3D) parts. In each build cycle, (1) a recoater blade spreads a layer of metal powders with thickness 20 – 50 μm from the metal powder reservoir to the build platform, (2) a laser beam controlled by an X-Y scanning mirror selectively melts a two-dimensional (2-D) pattern at the *xy* plane, (3) the part and build platform move downward to accommodate a new layer of material, and the powder platform moves upward to supply a new layer of metal powders. DMLS is capable of building complex parts with relatively low cost in a low-volume production setting (1 – 1,000 units [2]), and best fitted for the low-volume, high value-added aerospace and medical industries [2–13].

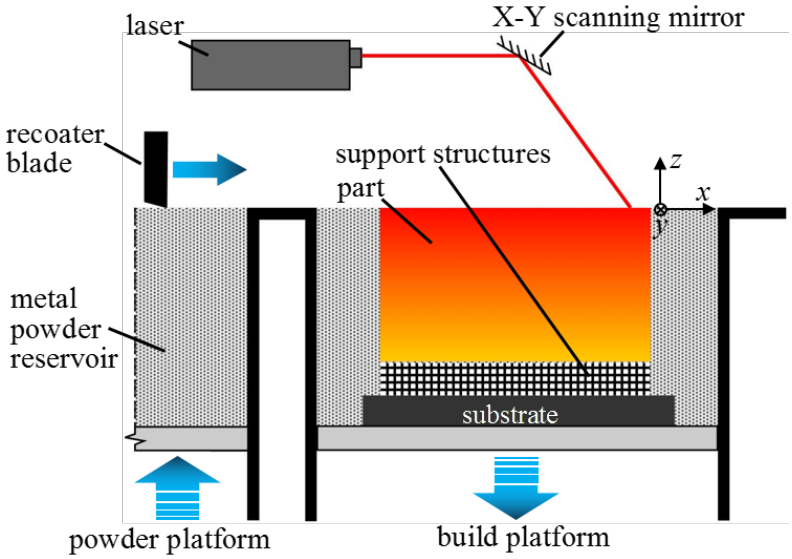

Figure 1. An example of direct metal laser sintering (DMLS) system.

Thermal distortion induced by the high thermal gradient in DMSL (~ 500°C/mm [14]) is a major challenge in current DMLS processes [15–18]. Moreover, the thermal distortion may even cause the failure of the entire process if the recoater blade crashes onto the distorted part [19]. The thermal distortion can be reduced by proper selection of the part orientation and the sacrificial support structures [20–26]. In this study, the support structures are dependent on the build orientation. In other words, once the build orientation is chosen, block-type support structures [19] are generated for overhanging surfaces with less than 35 degrees [27] to the substrate and for all surfaces below 10% of the total part height. As such, optimization of both build orientation and support structures boils down to only optimization of only build orientation in DMLS.

Optimization of build orientation for AM process has long been studied. Early studies were focused on enhancing the part quality, and reducing build cost and build time by considering the geometric influence of the build orientation, such as the part height, the volume of the support structures, the contact areas between the support and the part, the surface roughness due the staircase effect and the volumetric error [28–37]. Different from the previous approaches, Ulu and et al. [38] optimized the build orientation with a new objective function – the stress-based factor of safety. They calculated the stress tensor field by conducting a finite-element simulation with the orthotropic material assumption and a fixed boundary/loading condition. To the best of the authors' knowledge, however, no one has conducted optimization of build orientation to minimize the thermal distortion in AM build process. This is probably due to lack of efficient part-scale AM modeling tools which can predict thermal distortion.

In our previous studies, efficient part-scale thermal and thermo-mechanical models are developed to predict part distortion in DMLS AM [39,40]. To expedite the simulation speed, the thermal model took a novel paradigm different from existing finite element models. It breaks the part and support structures into a network of thermal capacitance and resistance, and the layer-by-layer build cycles of DMLS are modeled by adding new capacitance and resistance into the network. With temperature history calculated from the thermal model, the thermo-mechanical model predicted thermal contraction and thermal stresses accumulated in each build cycle. Each

build cycle is treated as a quasi-static thermo-mechanical process where only stresses at the end of each build cycle is calculated. Moreover, the thermo-mechanical model also simulated the support-removal process and the off-substrate part distortion can be predicted. The thermal and thermo-mechanical models can predict thermal distortion in the order of minutes, and can be integrated into optimization algorithms to find the optimal build orientation with minimum thermal distortion.

The rest of the manuscript is arranged as follows. Section 2 discussed the optimization algorithm used in this study and the generic objective function of thermal distortion. Section 3 discussed the constraints applied to the optimization. Section 4 presented two cases studies on a simple rectangle bar and an orthopedic handle part. Section 5 gave the conclusion and the potential future research.

2. Optimization methodology

2.1.DIRECT method

Because thermal distortion in DMLS cannot be explicitly expressed as a function of build orientation and calculating derivative numerically by evaluating the thermal/thermo-mechanical models multiple times is time-consuming, derivative-free optimization algorithms are more appropriate for optimizing build orientation in DMLS. Existing derivative-free optimization methods used for build orientation optimization include genetic algorithm [31,35], multi-objective genetic algorithm [34] and multi-criteria GA-based Pareto optimization [36].

DIRECT optimization algorithm is one type of derivative-free algorithm first introduced in [41], which is capable of solving difficult global optimization problems with bound constraints and real-valued objective function. The history and development of DIRECT method is discussed in [42]. The name DIRECT is short for “DIviding RECTangles” because the DIRECT algorithm keeps dividing the current domain into new hyper-rectangles and identifying potentially optimal hyper-rectangles from the new hyper-rectangles. Figure 2 shows the first three iterations of the DIRECT algorithm [43]. At the beginning of the first iteration, or initialization of the algorithm the search domain is divided along all dimensions. Note that the division starts with the dimension with the best function value so that the best function value is left in the largest space. Then the potentially optimal hyper-rectangles are found by applying the lemmas developed from the Lipschitzian optimization [43]. Next, the potentially optimal hyper-rectangles are divided along the longest dimension. If the lengths along all dimension are the same, the optimal hyper-rectangles are divided along all dimensions, starting with the dimension with the best function value, as what we did in the initialization. The optimization algorithm keeps finding new potentially optimal hyper-rectangles and dividing those hyper-rectangles until the maximum number of divisions is reached.

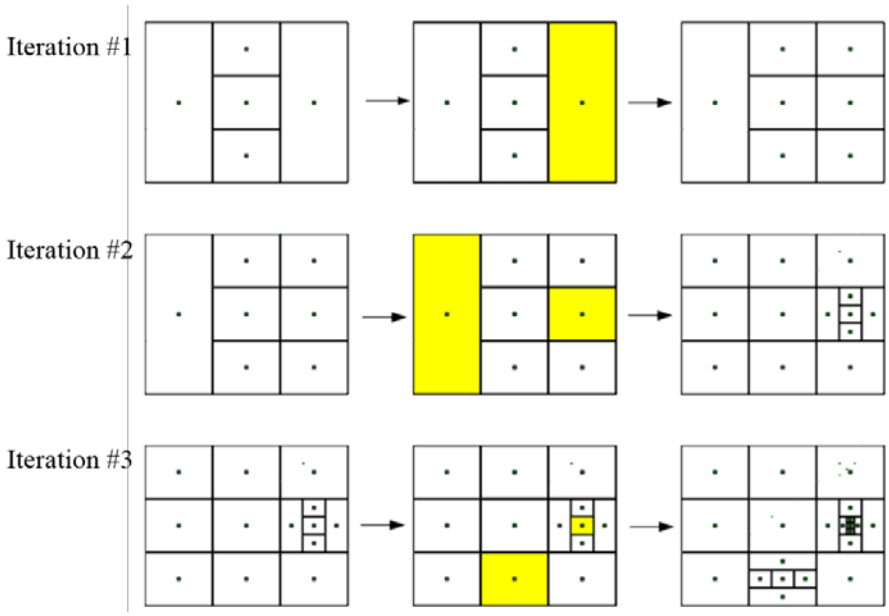

Figure 2. The schematic of the initial three iterations of the DIRECT optimization algorithm (adapted from [43]).

The DIRECT optimization algorithm was coupled with our DMLS thermal/thermo-mechanical model to optimize build orientation as shown in Fig. 3. In each optimization iteration, DIRECT passes a few potentially optimal build orientations to the DMLS models. The DMLS models generate support structure and predict the thermal distortion for those build orientations. Then values of the objective function are passed back to DIRECT. Based on the values of the objective function, DIRECT finds new potentially optimal build orientations. In this study, the build orientation is represented by part rotation about the *x* and *y* axes. It is assumed that the part rotation about *z* axis has no influence on the thermal distortion because the detailed scanning pattern of the laser beam is not considered in this study. For a generic part without symmetric features, the bound of the rotation angle is from -180 to 180 degrees.

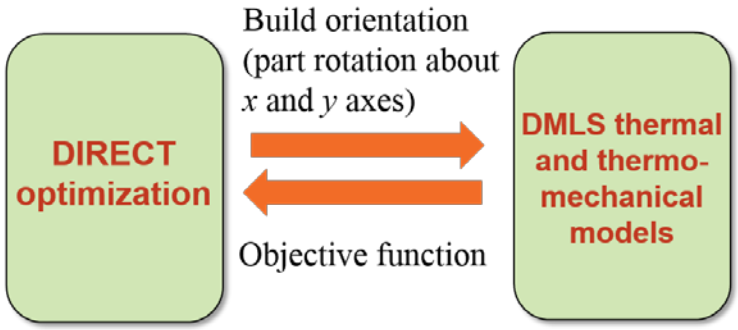

Figure 3. DIRECT algorithm applied to optimization of build orientation in DMLS.

2.2.Objective function

Displacement cannot be used as the generic objective function of thermal distortion in DMLS

because displacement of parts in DMLS depends on the boundary conditions applied in the stress relaxation period. Figures 4(a) and (b) show the displacement of a disk with diameter 45 mm and thickness 5 mm, and with boundary condition (BC) applied to the center and the edge of the disk. When BC is at the disk center, the edge of the disk bends upward and makes a "bowl" shape, as shown in Fig. 4(a); when BC is at the edge, the displacement near the BC is small and the displacement increases in areas away from the BC. However, the thermal distortion in Figs. 4(a) and (b) should be the same and with proper rotational and translational movement, the displacement in Figs. 4(a) and (b) should also match.

In this study a generic objective function is proposed by fitting the distorted part to the original part shape with nonlinear regression. Assume the nodal coordinates of the original and distorted part mesh are

$$X = \begin{bmatrix} x_1 & y_1 & z_1 \\ x_2 & y_2 & z_2 \\ \vdots & \vdots & \vdots \\ x_m & y_m & z_m \end{bmatrix} \text{and } \tilde{X} = \begin{bmatrix} \tilde{x}_1 & \tilde{y}_1 & \tilde{z}_1 \\ \tilde{x}_2 & \tilde{y}_2 & \tilde{z}_2 \\ \vdots & \vdots & \vdots \\ \tilde{x}_m & \tilde{y}_m & \tilde{z}_m \end{bmatrix}, \tag{1}$$

where m is the total number of nodes in the part mesh. Now rotate the distorted part mesh about x, y and z with angle α, β and γ, and move the distorted part mesh along vector (x_0, y_0, z_0). After the rotational and translational movement, the coordinates of the distorted part mesh are

$$\hat{X} = \left(R\tilde{X}^T\right)^T + T \tag{2}$$

where

$$R = R_x R_y R_z = \begin{bmatrix} 1 & 0 & 0 \\ 0 & \cos\alpha & -\sin\alpha \\ 0 & \sin\alpha & \cos\alpha \end{bmatrix} \begin{bmatrix} \cos\beta & 0 & \sin\beta \\ 0 & 1 & 0 \\ -\sin\beta & 0 & \cos\beta \end{bmatrix} \begin{bmatrix} \cos\gamma & -\sin\gamma & 0 \\ \sin\gamma & \cos\gamma & 0 \\ 0 & 0 & 1 \end{bmatrix}; \tag{3}$$

$$T = \begin{bmatrix} x_0 & y_0 & z_0 \\ \vdots & \vdots & \vdots \\ x_0 & y_0 & z_0 \end{bmatrix}_{m\times 3}. \tag{4}$$

Here we define the residual function as

$$S\left(X, \tilde{X}, \boldsymbol{\beta}\right) = \frac{1}{m}\sum_{i=1}^{m}\left(r_{xi}^2 + r_{yi}^2 + r_{zi}^2\right) \tag{5}$$

where $\boldsymbol{\beta} = \left[\alpha, \beta, \gamma, x_0, y_0, z_0\right]^T$ and $r = \hat{X} - X = \begin{bmatrix} r_{x1} & r_{y1} & r_{z1} \\ \vdots & \vdots & \vdots \\ r_{xi} & r_{yi} & r_{zi} \\ \vdots & \vdots & \vdots \end{bmatrix}_{m\times 3}$. The minimum residual is found at zero gradient

$$\frac{\partial S}{\partial \beta_j} = \frac{2}{m}\sum_{i=1}^{m}\left(r_{xi}\frac{\partial r_{xi}}{\partial \beta_j} + r_{yi}\frac{\partial r_{yi}}{\partial \beta_j} + r_{zi}\frac{\partial r_{zi}}{\partial \beta_j}\right) = 0 \quad (j = 1, \ldots, 6). \tag{6}$$

This is a nonlinear regression problem and $\boldsymbol{\beta}$ is refined iteratively with

$$\boldsymbol{\beta}^{k+1} = \boldsymbol{\beta}^{k} + \Delta\boldsymbol{\beta} \tag{7}$$

where

$$\begin{aligned}
&\Delta\boldsymbol{\beta} = -\left(\mathbf{J}^{xT}\mathbf{J}^{x} + \mathbf{J}^{yT}\mathbf{J}^{y} + \mathbf{J}^{zT}\mathbf{J}^{z}\right)^{-1}\left(\mathbf{J}^{xT}\mathbf{r}_{x} + \mathbf{J}^{yT}\mathbf{r}_{y} + \mathbf{J}^{zT}\mathbf{r}_{z}\right) \\
&\mathbf{r}_{x} = r_{xi},\ \mathbf{r}_{y} = r_{yi},\ \text{and}\ \mathbf{r}_{z} = r_{zi} \\
&\mathbf{J}^{x} = J_{ij}^{x} = \frac{\partial r_{xi}}{\partial \beta_{j}},\ \mathbf{J}^{y} = J_{ij}^{y} = \frac{\partial r_{yi}}{\partial \beta_{j}},\ \text{and}\ \mathbf{J}^{z} = J_{ij}^{z} = \frac{\partial r_{zi}}{\partial \beta_{j}}
\end{aligned} \tag{8}$$

The iteration stops at

$$\frac{\left\|\boldsymbol{\beta}^{k+1} - \boldsymbol{\beta}^{k}\right\|}{\left\|\boldsymbol{\beta}^{k}\right\|} < 10^{-6}. \tag{9}$$

The minimum residual $S_{\min}$ is used as the generic objective function in DIRECT, and $S_{\min}$ represents the average thermal distortion in the part. Figure 4(c) shows the history of the residual and the *z*-displacement after the nonlinear regression. It is worth noting that the two BCs shown in Figs. 4(a) and (b) give the same minimum residual $S_{\min}$.

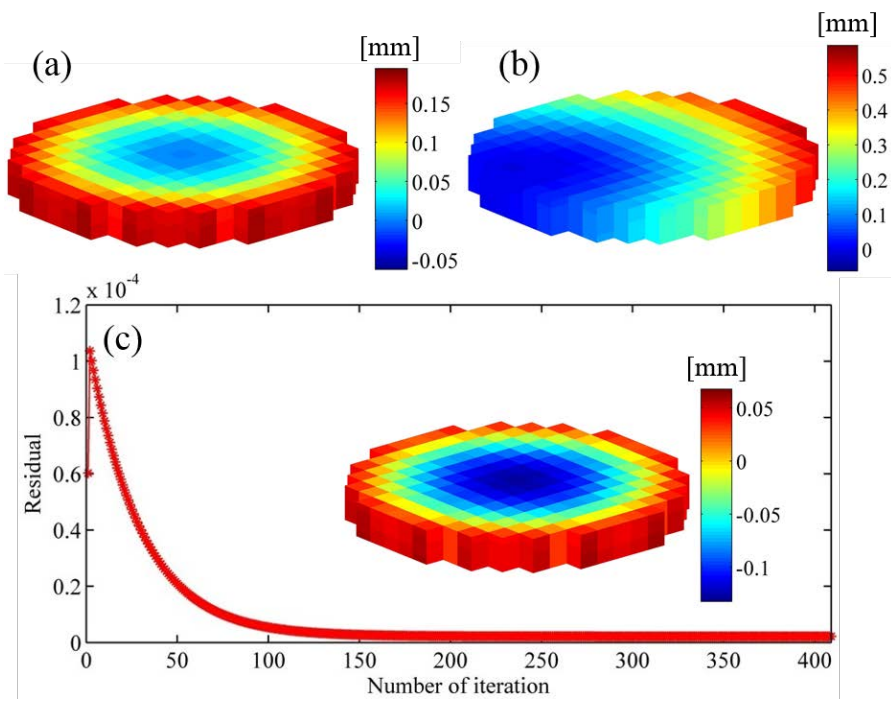

Figure 4. Simulated off-substrate *z*-displacement of a disk with diameter 45 mm and thickness 5 mm built with DMLS with boundary condition applied to (a) the center and (b) the edge. (c) Generic objective function of thermal distortion and *z*-displacement after the nonlinear regression.

2.3.Constraints

2.3.1. Temperature constraint

To avoid overheating of the sintering plane, a temperature constraint must be applied. Figure 5 shows the simulated temperature history of a rectangular bar built vertically in DMLS. As more materials are deposited onto the part during the build, the thermal resistance and thermal mass increase and the temperature decay rates decrease. Without proper thermal management, the top

sintering plane will remain in liquid phase when the next build cycle starts. The temperature constraint is implemented in DIRECT algorithm as follows. At the end of each build cycle, if the average temperature of the top superlayer is higher than the solidus temperature, a feasible flag will be set to 1 (default value 0) and returned to the DIRECT algorithm. As such, DIRECT will not choose the current build orientation as the potentially optimal orientation even if the thermal distortion is small.

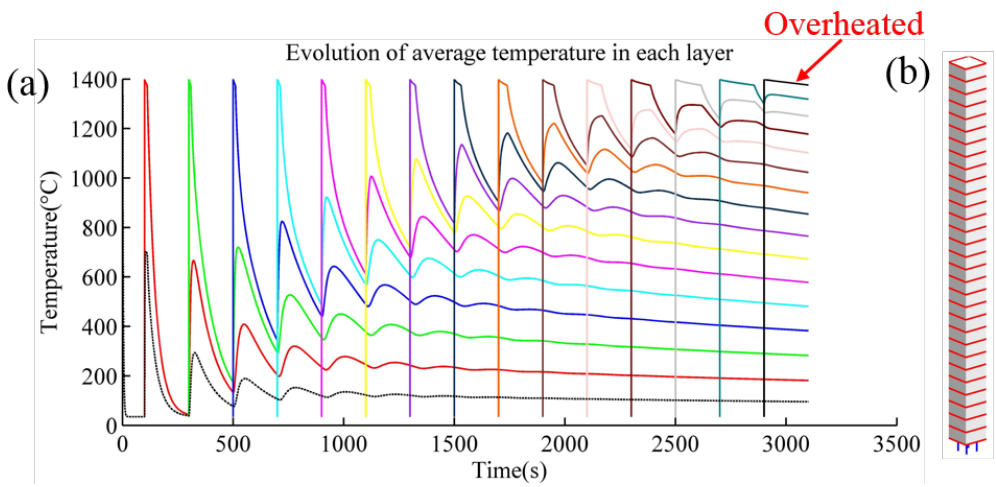

Figure 5. (a) Simulated temperature history of each superlayer of a rectangular bar built vertically in DMLS. (b) The rectangular bar sliced into superlayers for thermal analysis.

2.3.2. Oxidation constraint

Another constraint is applied to the oxidation in DMLS. Due to high build temperature, oxidation is not avoidable in DMLS. However, by controlling the build temperature, the oxidation film thickness can be controlled in an acceptable level. The parabolic law of oxidation is widely used to predict the accumulation of oxidation film on metal alloys [44–46]. The law was also applied to study the oxidation in LENS additive manufacturing process [47]. The parabolic law is expressed as

$$x^2 = k_p t\,, \tag{10}$$

where x is the layer thickness, t is time and k_p is the oxidation rate constant. The oxidation rate constant can be expressed in Arrhenius form as

$$k_p = k_0 \exp\left(-\frac{E}{RT}\right), \tag{11}$$

where E is activation energy, T is temperature in Kelvin and R is gas constant. The oxidation rate constant for stainless steel is [45]

$$k_p = 1.02\times10^3 \exp\left(-\frac{16.44\times10^3}{T}\right). \tag{12}$$

It is customary to give k_p in the form of weight increase and in Eq. (12) the unit of k_p is $g^2m^{-4}s^{-1}$ with the assumption that the oxide density is $5\times10^6 gm^{-3}$. The oxidation rate constant is very sensitive to temperature change. When temperature is below 700 °C, the oxidation rate constant is

near zero while the oxidation rate increases exponentially as temperature increases above 1000 °C.

With the temperature history predicted by our thermal model, the evolution of oxidation rate constants at each superlayer are available with Eq. (12). By integrating the parabolic law of oxidation over the history of DMLS build process, the final oxidation film thicknesses at each superlayer can be obtained. However, because our thermal model assumed that laser heat fluxes are applied to the entire thick superlayer (large thermal mass), the top superlayer in the simulation stay at high temperature longer than the top layer in the experiment. As such, the oxidation level predicted by our thermal model is higher than the real oxidation, and needs to be calibrated against experiment data.

Due to the interference of light waves, oxidation films with different layer thickness exhibit different colors. Thus, the oxidation film thickness can be estimated from the interface color of the oxidation film. Figure 6 shows the interface color of stainless steel oxidation film changes from brown to green as the oxidation film thickness increases from ~80 nm to ~450 nm [44]. Based on Fig. 6, we estimate that in our experiment the oxidation film is negligibly small when the rectangular bar is built horizontally, and the oxidation film thickness is ~80 nm when built with 45 degrees to the substrate. To match the oxidation level predicted by the simulation to the oxidation level in the experiment, a calibration factor of 50 is chosen. After dividing the oxidation film thickness from the parabolic law of oxidation in Eq. (10) by the calibration factor, the predicted oxidation film thickness is 9 nm for the bar built horizontally and 94 nm for the bar built with 45 degree, consistent with the experimental observation.

The oxidation constraint is implemented in DIRECT algorithm as follows. After the temperature history in DMLS is predicted by our thermal model, the maximum oxidation film thickness in the part obtained. If the maximum oxidation film thickness is higher than a user-defined threshold value, the feasible flag will be set to 1 (default value 0) and returned to the DIRECT algorithm. As such, DIRECT will not choose the current build orientation as the potentially optimal orientation even if the thermal distortion is small.

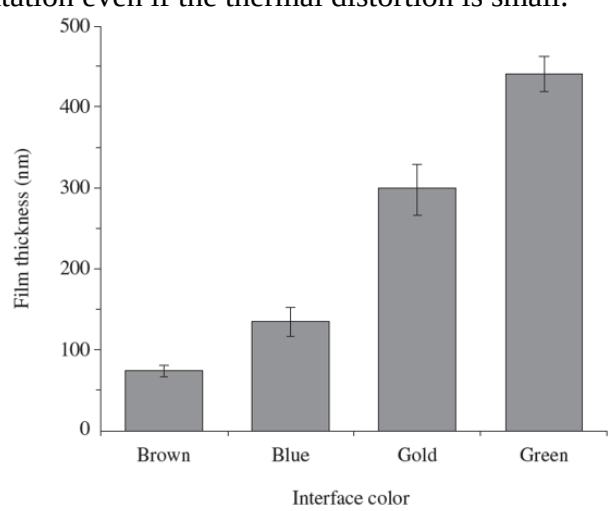

Figure 6. Interface color of stainless steel oxidation film with various film thickness.

3. Case studies

3.1.Rectangular bar

First, the build orientation of the 316L stainless bar (10×10×150 mm) is optimized for minimum thermal distortion. Two different threshold values of the maximum oxidation film thickness, 120 nm and 20 nm, are tested. Figure 7(a) shows the history of the potentially optimal (blue curve) and optimal (red curve) values of the objective function when the threshold value of the maximum oxidation film thickness is 120 nm. The maximum number of build orientations to be evaluated is set to be 100. Nevertheless, the DIRECT algorithm typically evaluates more build orientations than the specified number. Figure 7(b) shows the optimal build orientation of the rectangular bar. The build orientation is achieved by rotating a horizontal bar about *y* axis with -80 degrees and then about *x* axis with -35.6 degrees. The objective function at this optimal build orientation is 9.5×10^{-10} m^2 and the maximum oxidation thickness is 94 nm. It takes about 13 hours to finish the optimization. Figure 7(c) shows the experimental results. The build is successful at the first trial. By referring to the interface color shown in Fig. 6, it can be estimated that the thickness of the oxidation layer is about 100 nm, consistent with our simulation results.

Figure 8 shows the optimization results when the threshold value of the maximum oxidation layer thickness is set to 20 nm. It takes about 8 hours to finish the optimization. Figure 8(a) shows the history of the potentially optimal and optimal values of the objective function. Because the threshold value of the maximum oxidation layer thickness is pretty low, most of the build orientations give a much higher oxidation layer thickness. Under those circumstances, the DIRECT assigns a high value (typically 1×10^9) to the objective function, regardless of the real objective function value at the build orientation. As such, the build orientations not satisfying the oxidation constraint can be ruled out. Out of the ~100 build orientations, only a few build orientations satisfy the oxidation constraint, as shown by Fig. 8(a). Figure 8(b) shows the optimal build orientation, which is achieved by rotating the horizontal bar about $\underline{x}$ axis with 80 degrees. The optimal build orientation is close to the horizontal build such that heat can be dissipated quickly to decrease the oxidation level. The maximum oxidation film thickness under this build orientation is 16 nm from the simulation.

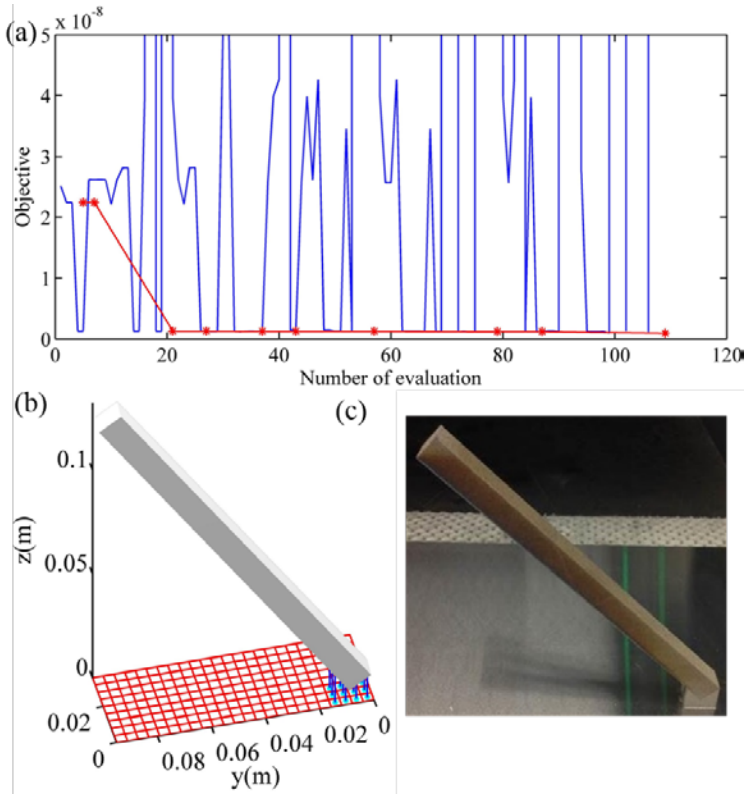

Figure 7. Optimization of a rectangular bar (10×10×150 mm) with maximum oxidation film thickness threshold of 120 nm. (a) History of potentially optimal value of the objective function (blue curve) and optimal value of the objective function (red curve). (b) Optimal build orientation. (c) The rectangular bar build with the optimal build orientation.

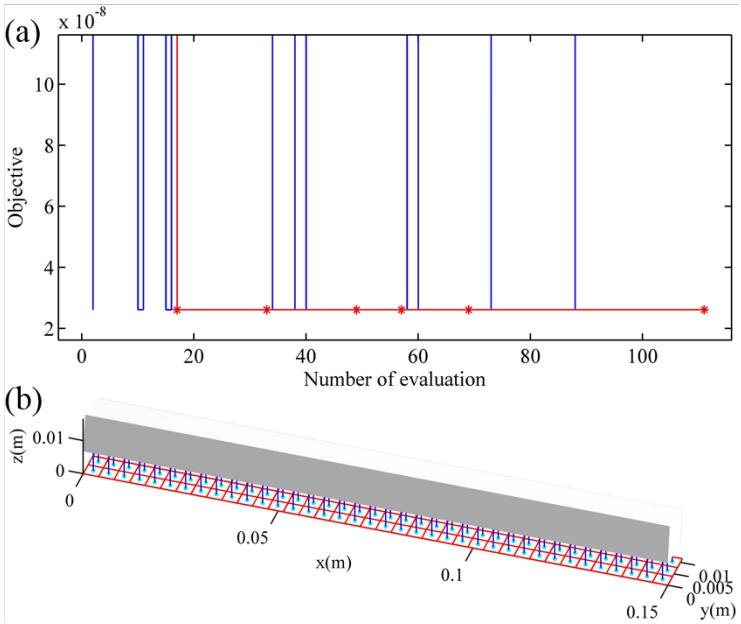

Figure 8. Optimization of a rectangular bar (10×10×150 mm) with maximum oxidation film thickness threshold of 20 nm.

Figure 9 shows the off-substrate distortion at the top surface of the rectangular bar measured by the coordinate measuring machine (CMM). Figure 9(a) shows the distortion for the horizontal build orientation chosen by an invoice operator and Fig. 9(b) shows the distortion at the optimal build orientation indicated by Fig. 7(b). When built horizontally, the rectangular bent upward and the highest and lowest locations are marked by red points (see Fig 9(a)). The vertical distance between the two red points, termed with flatness, is 447 μm. Similarly, when built with the optimal orientation, the bar shows insignificant distortion. The vertical distance between the highest and lowest points is 109 μm, a reduction of 75.6% in comparison to the horizontal build orientation. Moreover, the surface roughness is the main reason for the flatness of 109 μm, as shown by Fig. 9(b).

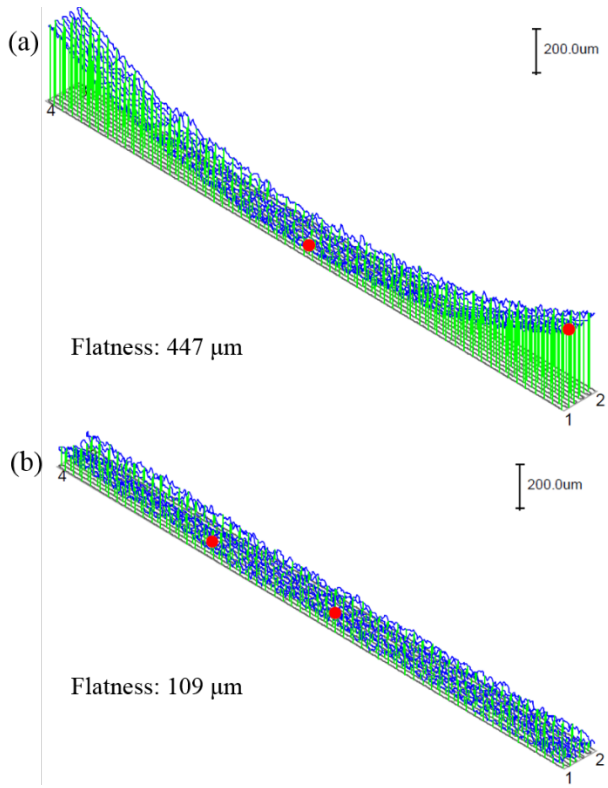

Figure 9. Off-substrate distortion at the top surface of the rectangular bar built with (a) horizontal build orientation chosen by the novice operator and (b) the optimal build orientation as shown in Fig. 7.

3.2.Handle for orthopedic application

Hereafter, the DIRECT optimization algorithm is applied to a generic orthopedic handle. The maximum number of build orientations to be evaluated is 100 and the threshold value of the maximum oxidation film thickness is set to 120 nm. It takes about 22 hours to finish the optimization. Figure 10(a) shows the history of the potentially optimal (blue curve) and optimal (red curve) values of the objective function, and Fig. 10(b) shows the optimal build orientation. The larger end of the handle is oriented to the bottom side and in contact with support structures so that heat can be dissipated efficiently. The remaining part is built with no support, resembling the optimal build orientation of the rectangular bar shown in Fig. 7(b). The maximum oxidation film thickness is 49 nm with the optimal build orientation. Figure 10(c) shows the build of the

handle in the EOS M290 machine. The build is successful at the first trial.

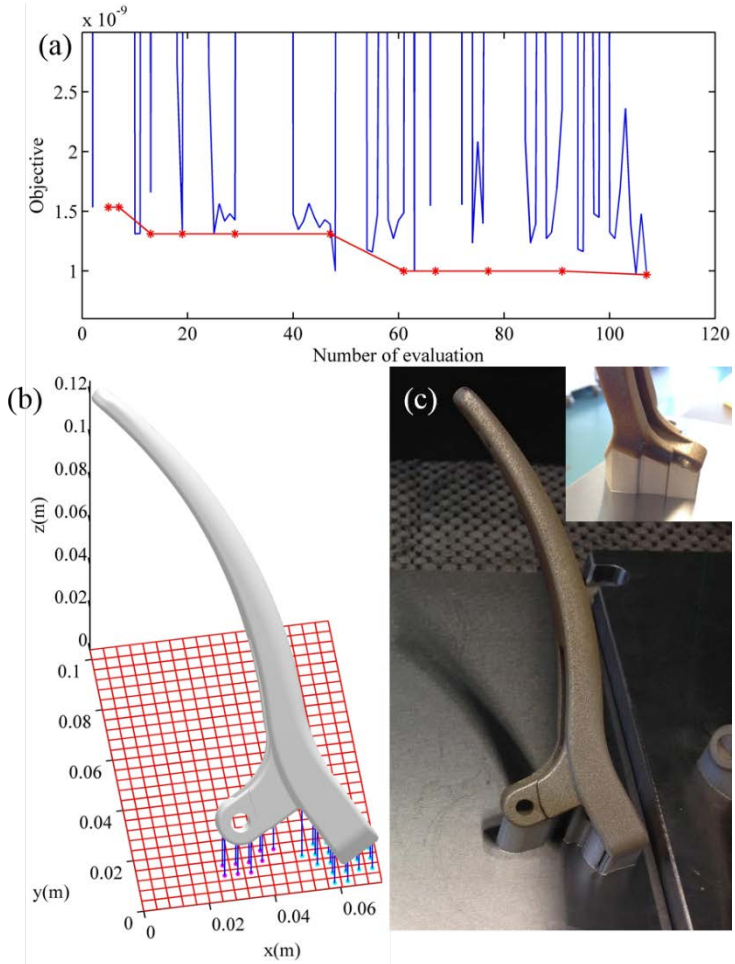

Figure 10. Optimization of an orthopedic handle with maximum oxidation film thickness threshold of 120 nm. (a) History of potentially optimal value of the objective function (blue curve) and optimal value of the objective function (red curve). (b) Optimal build orientation. (c) The orthopedic handle build with the optimal build orientation.

Figure 11 shows the off-substrate distortion at the top surface of the handle built with horizontal build orientation chosen by the novice operator and the optimal build orientation indicated by Fig. 10. The off-substrate distortion of the horizontally built handle was measured by fixing the origin as shown by the axes. The maximum displacement at the tip of the handle is as high as 3.5 mm. However, the distortion is significant reduced under the optimal build orientation as shown by Fig. 10(b).

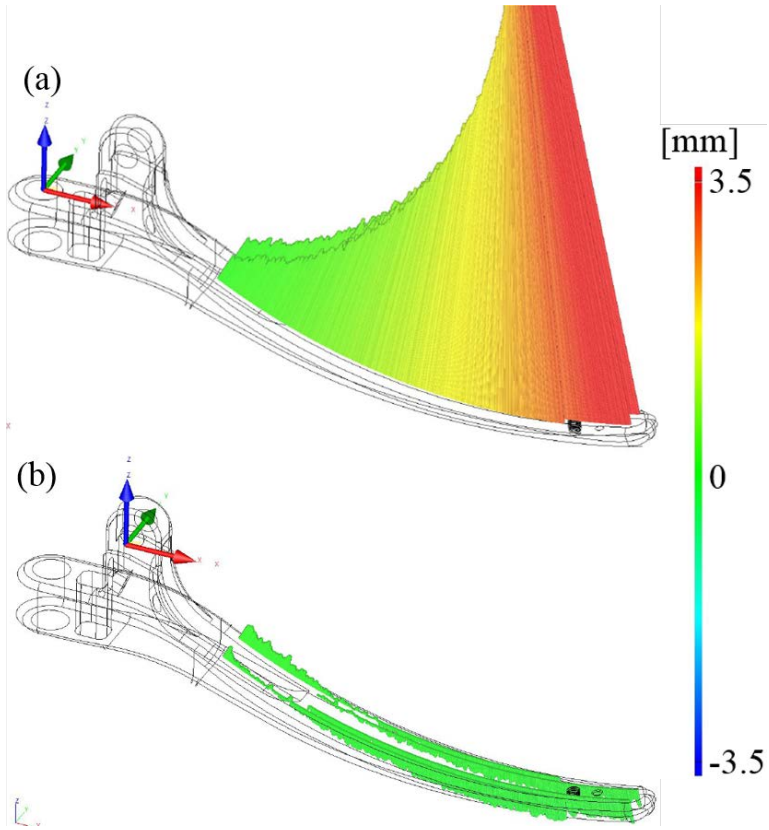

Figure 11. Off-substrate distortion at the top surface of the orthopedic handle built with (a) horizontal build orientation chosen by the novice operator and (b) the optimal build orientation as shown in Fig. 10.

4. Conclusion and future research

On the foundation of the coupled thermal and thermo-mechanical models developed in our previous work, this manuscript presents an optimization algorithm for minimum thermal distortion in the DMLS AM process. The DIRECT search method is used with a universal objective function for thermal distortion. Both a thermal and an oxidation constraints are applied to rule out build orientations resulting in overheating or too much oxidation. The optimization algorithm was first applied to a simple rectangular bar and then to a generic orthopedic handle. On average it takes about 15 hours to finish each optimization. The rectangular bar and the handle with the optimal build orientations were built in an EOS M290 machine and the distortion of the parts was measured by a coordinate measuring machine. In comparison to intuitive build orientations chosen by our two novice operators, the optimized build orientations gave about 70% reduction on the thermal distortion. The future work will focus on coupled optimization of build orientation and support structure design for minimum thermal distortion. The heuristics for support structure generation in this study will not be used any longer. As such, the support structures will become independent of build orientations and need to be optimized independently. Topology optimization is a tentative approach for support optimization. Parameters of support structure such as teeth length, hatch distance and fragmentation should also be included into the optimization algorithm.

References

[1] Standard Terminology for Additive Manufacturing Technologies, (Withdrawn 2015), (2015).

[2] W. Frazier, Metal Additive Manufacturing: A Review, J. Mater. Eng. Perform. 23 (2014) 1917–1928. doi:10.1007/s11665-014-0958-z.

[3] D.D. Gu, W. Meiners, K. Wissenbach, R. Poprawe, Laser additive manufacturing of metallic components: materials, processes and mechanisms, Int. Mater. Rev. 57 (2012) 133–164. doi:10.1179/1743280411y.0000000014.

[4] I. Gibson, D.W. Rosen, B. Stucker, Additive Manufacturing Technologies: Rapid Prototyping to Direct Digital Manufacturing, Springer US, 2009. https://books.google.com/books?id=jcFs0VVi9OAC.

[5] K.P. Karunakaran, A. Bernard, S. Suryakumar, L. Dembinski, G. Taillandier, Rapid manufacturing of metallic objects, Rapid Prototyp. J. 18 (2012) 264–280. doi:10.1108/13552541211231644.

[6] L.E. Murr, S.M. Gaytan, D.A. Ramirez, E. Martinez, J. Hernandez, K.N. Amato, P.W. Shindo, F.R. Medina, R.B. Wicker, Metal Fabrication by Additive Manufacturing Using Laser and Electron Beam Melting Technologies, J. Mater. Sci. Technol. 28 (2012) 1–14. doi:10.1016/s1005-0302(12)60016-4.

[7] B. Vayre, F. Vignat, F. Villeneuve, Metallic additive manufacturing: state-of-the-art review and prospects, Mech. Ind. 13 (2012) 89–96. doi:10.1051/meca/2012003.

[8] X. Gong, T. Anderson, K. Chou, Review on powder-based electron beam additive manufacturing technology, Manuf. Rev. 1 (2014) 2. doi:10.1051/mfreview/2014001.

[9] M. Shellabear, O. Nyrhilä, DMLS-Development history and state of the art, in: 2004.

[10] H.M. Chae, A numerical and experimental study for residual stress evolution in low alloy steel during laser aided additive manufacturing process, University of Michigan, 2013.

[11] W. King, A.T. Anderson, R.M. Ferencz, N.E. Hodge, C. Kamath, S.A. Khairallah, Overview of modelling and simulation of metal powder bed fusion process at Lawrence Livermore National Laboratory, Mater. Sci. Technol. 31 (2015) 957–968. doi:10.1179/1743284714Y.0000000728.

[12] N.P. Lavery, S.G.R. Brown, J. Sienz, J. Cherry, F. Belblidia, A review of Computational Modelling of Additive Layer Manufacturing-multi-scale and multi-physics, in: 2014.

[13] M. Megahed, H.-W. Mindt, N. N'Dri, H. Duan, O. Desmaison, Metal additive-manufacturing process and residual stress modeling, Integrating Mater. Manuf. Innov. 5 (2016) 1–33. doi:10.1186/s40192-016-0047-2.

[14] K. Zeng, D. Pal, H.J. Gong, N. Patil, B. Stucker, Comparison of 3DSIM thermal modelling of selective laser melting using new dynamic meshing method to ANSYS, Mater. Sci. Technol. 31 (2015) 945–956. doi:10.1179/1743284714y.0000000703.

[15] P. Aggarangsi, J.L. Beuth, Localized Preheating Approaches for Reducing Residual Stress in Additive Manufacturing, in: 2006.

[16] D. Buchbinder, W. Meiners, N. Pirch, K. Wissenbach, J. Schrage, Investigation on reducing distortion by preheating during manufacture of aluminum components using selective laser

melting, J. Laser Appl. 26 (2014) 012004. doi:10.2351/1.4828755.
[17] N. Shen, K. Chou, Numerical Thermal Analysis in Electron Beam Additive Manufacturing with Preheating Effects, in: 2012.
[18] I. Yadroitsava, I. Yadroitsev, Residual stress in metal specimens produced by direct metal laser sintering, (2015).
[19] T.A. Krol, M.F. Zaeh, C. Seidel, Optimization of Supports in Metal-Based Additive Manufacturing by Means of Finite Element Models, (2012).
[20] K. Zeng, Optimization of Support Structures for Selective Laser Melting, University of Louisville, 2015.
[21] O. Poyraz, E. Yasa, G. Akbulut, A. Orhangul, S. Pilatin, Investigation of Support Structures for Direct Metal Laser Sintering (DMLS) Of In625 Parts, in: 2015.
[22] J.-P. Järvinen, V. Matilainen, X. Li, H. Piili, A. Salminen, I. Mäkelä, O. Nyrhilä, Characterization of Effect of Support Structures in Laser Additive Manufacturing of Stainless Steel, Phys. Procedia. 56 (//) 72–81. doi:10.1016/j.phpro.2014.08.099.
[23] F. Calignano, Design optimization of supports for overhanging structures in aluminum and titanium alloys by selective laser melting, Mater. Des. 64 (12) 203–213. doi:10.1016/j.matdes.2014.07.043.
[24] A. Hussein, L. Hao, C. Yan, R. Everson, P. Young, Advanced lattice support structures for metal additive manufacturing, J. Mater. Process. Technol. 213 (7) 1019–1026. doi:10.1016/j.jmatprotec.2013.01.020.
[25] T.A. Krol, M.F. Zaeh, C. Seidel, Optimization of Supports in Metal-Based Additive Manufacturing by Means of Finite Element Models, (2012).
[26] T.A. Krol, M.F. Zah, J. Schilp, C. Seidel, C. Groth, Computational-Efficient Design of Support Structures and Material Modeling for Metal-Based Additive Manufacturing, in: 2011.
[27] G. Strano, L. Hao, R.M. Everson, K.E. Evans, A new approach to the design and optimisation of support structures in additive manufacturing, Int. J. Adv. Manuf. Technol. 66 (2013) 1247–1254. doi:10.1007/s00170-012-4403-x.
[28] P. Alexander, S. Allen, D. Dutta, Part orientation and build cost determination in layered manufacturing, Comput.-Aided Des. 30 (4) 343–356. doi:10.1016/S0010-4485(97)00083-3.
[29] S.H. Choi, S. Samavedam, Modelling and optimisation of Rapid Prototyping, Comput. Ind. 47 (1) 39–53. doi:10.1016/S0166-3615(01)00140-3.
[30] S.H. Masood, W. Rattanawong, A Generic Part Orientation System Based on Volumetric Error in Rapid Prototyping, Int. J. Adv. Manuf. Technol. 19 (2002) 209–216. doi:10.1007/s001700200015.
[31] H.S. Byun, K.H. Lee, Determination of the optimal part orientation in layered manufacturing using a genetic algorithm, Int. J. Prod. Res. 43 (2005) 2709–2724. doi:10.1080/00207540500031857.
[32] P.M. Pandey, N. Venkata Reddy, S.G. Dhande, Part deposition orientation studies in layered manufacturing, J. Mater. Process. Technol. 185 (4) 125–131. doi:10.1016/j.jmatprotec.2006.03.120.
[33] S. Danjou, P. Koehler, Determination of Optimal Build Direction for Different Rapid

Prototyping Applications, in: 2009.
[34] A.S. Nezhad, M. Vatani, F. Barazandeh, A.R. Rahimi, Determining the optimal build directions in layered manufacturing, WSEAS Trans. Appl. Theor. Mech. 4 (2009) 185–194.
[35] A.M. Phatak, S.S. Pande, Optimum part orientation in Rapid Prototyping using genetic algorithm, J. Manuf. Syst. 31 (10) 395–402. doi:10.1016/j.jmsy.2012.07.001.
[36] Y. Li, J. Zhang, Multi-criteria GA-based Pareto optimization of building direction for rapid prototyping, Int. J. Adv. Manuf. Technol. 69 (2013) 1819–1831. doi:10.1007/s00170-013-5147-y.
[37] R. Paul, S. Anand, Optimization of layered manufacturing process for reducing form errors with minimal support structures, J. Manuf. Syst. (2014). doi:10.1016/j.jmsy.2014.06.014.
[38] E. Ulu, E. Korkmaz, K. Yay, O. Burak Ozdoganlar, L. Burak Kara, Enhancing the Structural Performance of Additively Manufactured Objects Through Build Orientation Optimization, J. Mech. Des. 137 (2015) 111713. doi:10.1115/1.4030998.
[39] H. Peng, D.B. Go, R. Billo, S. Gong, R. Shankar, B.A. Gatrell, J. Budzinski, P. Ostiguy, R. Attardo, C. Tomonto, J. Neidig, D. Hoelzle, Part-scale model for fast prediction of thermal distortion in DMLS additive manufacturing; Part 1: a thermal circuit network model, in: Austin, Texas, 2016.
[40] H. Peng, D.B. Go, R. Billo, S. Gong, R. Shankar, B.A. Gatrell, J. Budzinski, P. Ostiguy, R. Attardo, C. Tomonto, J. Neidig, D. Hoelzle, Part-scale model for fast prediction of thermal distortion in DMLS additive manufacturing; Part 2: a quasi-static thermo-mechanical model, in: Austin, Texas, 2016.
[41] D.R. Jones, C.D. Perttunen, B.E. Stuckman, Lipschitzian optimization without the Lipschitz constant, J. Optim. Theory Appl. 79 (1993) 157–181. doi:10.1007/bf00941892.
[42] R.M. Lewis, V. Torczon, M.W. Trosset, Direct search methods: then and now, J. Comput. Appl. Math. 124 (January 12) 191–207. doi:10.1016/S0377-0427(00)00423-4.
[43] D.E. Finkel, DIRECT Optimization Algorithm User Guide, (2003). http://www4.ncsu.edu/~ctk/Finkel_Direct/.
[44] R.M.R. Junqueira, C.R. de O. Loureiro, M.S. Andrade, V.T.L. Buono, Characterization of interference thin films grown on stainless steel surface by alternate pulse current in a sulphochromic solution, Mater. Res. 11 (2008) 421–426.
[45] R.K. Wild, High temperature oxidation of austenitic stainless steel in low oxygen pressure, Corros. Sci. 17 (//) 87–104. doi:10.1016/0010-938X(77)90011-7.
[46] W.W. Smeltzer, Oxidation of aluminum in temperature range 400 degrees -600 degrees, J Electrochem Soc. (1956).
[47] R. Łyszkowski, High-Temperature Oxidation of Fe3Al Intermetallic Alloy Prepared by Additive Manufacturing LENS, Materials. 8 (2015) 1499–1512. doi:10.3390/ma8041499.